Synthesis, Reactivity, Electrochemical Study, and Crystal Structures of $(\eta^5:\eta^5\text{-}(C_5H_3CO_2Me)_2)Mo_2(CO)_6$

Salomé Delgado,*,† M. José Macazaga, Rosa M. Medina, and Consuelo Moreno

Departamento de Química Inorgánica, Universidad Autónoma de Madrid, Cantoblanco, 28049-Madrid, Spain

Jaime González-Velasco and M. Luisa Marcos

Departamento de Química, Universidad Autónoma de Madrid, 28049-Madrid, Spain

David H. Farrar and Ravindranath Ramachandran

Lash Miller Chemical Laboratories, University of Toronto, 80 St. George Street, Toronto, Ontario, Canada M5S 1A1

Received May 24, 1996[⊗]

The reaction of a dicarbomethoxydihydrofulvalene solution with $Mo(CO)_6$ leads to the formation of two isomers of $(\eta^5:\eta^5\text{-}(C_5H_3CO_2Me)_2)Mo_2(CO)_6$ (**1** and **2**). The X-ray structure of both compounds has been determined. Reaction of **2** with $LiEt_3BH$ yields $Li_2[(\eta^5:\eta^5\text{-}(C_5H_3CO_2Me)_2)Mo_2(CO)_6]$ (**3**), and this with $Hg(CN)_2$ results in the insertion of Hg into the Mo−Mo bond giving $(\eta^5:\eta^5\text{-}(C_5H_3CO_2Me)_2)Mo_2(CO)_6Hg$ (**4**). The electrochemical study of **1**−**4** is reported. The two-electron reduction of **1** and **2**, through an ECE mechanism, leads to the dianions. This reduction takes place at a significantly less negative potential than for the unsubstituted fulvalene $(\eta^5:\eta^5\text{-}C_{10}H_8)Mo_2(CO)_6$ (**5**) due to the electron-withdrawing properties of the carbomethoxy substituents. The oxidation of **1** and **2** is also affected by the substituents, taking place at a more positive potential than **5**. The reduction of **4** yields the dianion $\mathbf{2}^{2-}$ and liberates Hg.

Introduction

The chemistry of dinuclear organometallic complexes containing the fulvalene (Fv) ligand has recently become a topic of renewed interest.[1−6] Besides their interesting electrochemical[7,8] and magnetic[9] properties, the reactivities of Fv complexes should differ from those of their Cp analogues. There are at least two important reasons that suggest this difference. First, in the metal−metal-bonded complexes, the Fv ligands are forced away from planarity in order to accommodate the metal−metal bond. The distance between the ring centroids in a planar Fv ligand is ca. 4.0 Å.[10] In comparison, the Ru−Ru distance in $FvRu_2(CO)_4$ is 2.821 Å and the Fv ligand is distorted from planarity by a 28.5° dihedral angle between the two Cp ring planes.[11] Second, the conjugated π systems of the Fv ligand provide a mechanism for electronic communications between the metal centers regardless of whether a metal−metal bond is present or not and whether the metals are oriented syn or anti respect to the bridging ligand.

Few functionalized fulvalene complexes are known. To our knowledge, only complexes of 1,1′,3,3′-tetra-*tert*-butyl-5,5′-dihydropentafulvalene[12] (stabilized toward polymerization with Fe,[13] Cr, Mo, W,[14] and Tl[15]), the dimethyl derivative $(\eta^5:\eta^5\text{-}(C_5H_3Me)_2)W_2(CO)_6$[4] (obtained as a mixture of six possible stereoisomers) and the dibenzofulvalenes[16,17] have been recently synthesized. Also, a few ferrocene-based fulvalene-bridged heterobimetallic complexes have been prepared.[18−20] In this paper we describe the synthesis of two isomers of $(\eta^5:\eta^5\text{-}(C_5H_3CO_2Me)_2)Mo_2(CO)_6$ (**1** and **2**), their structural characterization, the lithium salt of isomer **2** (**3**), the reaction of **3** with $Hg(CN)_2$, yielding a new mercurial compound **4**, and the electrochemical behavior of **1**−**4** to evaluate the influence of the carbomethoxy substituent on the Fv ligand.

† E-mail: SDELGADO@CCUAM3.SDI.UAM.ES.

⊗ Abstract published in *Advance ACS Abstracts,* November 1, 1996.

(1) Drage, J. S.; Vollhardt, K. P. C. *Organometallics* **1986**, *5*, 280.
(2) McGovern, P. A.; Vollhardt, K. P. C. *Synlett* **1990,** 493.
(3) Boese, R.; Huffman, M. A.; Vollhardt, K. P. C. *Angew. Chem., Int. Ed. Engl.* **1991**, *30*, 1463.
(4) Tilset, M.; Vollhardt, K. P. C.; Boese, R. *Organometallics* **1994**, *13*, 3146.
(5) Herberhold, M.; Biersack, M.; Bitterwolf, T. E.; Rheingold, A. L. *Z. Naturforsch., B: Chem. Sci.* **1993**, *48* (2), 161.
(6) Kahn, A. P.; Boese, R.; Blümel, J.; Vollhardt, K. P. C. *J. Organomet. Chem.* **1994**, *472*, 149.
(7) Delville-Desbois, M.-H.; Brown, D. S.; Vollhardt, K. P. C.; Astruc, D. *J. Chem. Soc., Chem. Commun.* **1991,** 1355.
(8) Atwood, C. G.; Geiger, W. E. *J. Am. Chem. Soc.* **1993**, *115*, 5310.
(9) Hudeczek, P.; Köhler, F. H. *Organometallics* **1992**, *11*, 1773.
(10) (a) Smart, J. C.; Curtis, C. J. *Inorg. Chem.* **1977**, *16*, 1788. (b) Davis, J. H., Jr.; Sinn, E.; Grimes, R. N. *J. Am. Chem. Soc.* **1989**, *111*, 4784.
(11) Vollhardt, K. P. C.; Weidman, T. W. *J. Am. Chem. Soc.* **1983**, *105*, 1676.
(12) Brand, R.; Krimmer, H.-P.; Lindner, H.-J.; Sturm, V.; Hafner, K. *Tetrahedron Lett.* **1982**, *23*, 5153.
(13) Jutzi, P.; Schnittger, J.; Dahlhaus, J.; Gestmann, D.; Lene, H.-C. *J. Organomet. Chem.* **1991**, *415*, 117.
(14) Jutzi, P.; Schnittger, J. *Chem. Ber.* **1989**, *122*, 629.
(15) Jutzi, P.; Schnittger, J.; Hursthouse, M. B. *Chem. Ber.* **1991**, *124*, 1693.
(16) Kerber, R. C.; Waldbaum, B. *Organometallics* **1995**, *14*, 4742.
(17) Kerber, R. C.; Waldbaum, B. R. *Organometallics* **1996**, *513*, 277.
(18) Wan, S.; Begley, M. J.; Mountford, P. *J. Organomet. Chem.* **1995**, *489*, C28.
(19) Begley, M. J.; Mountford, P.; Stewart, P. J.; Swallow, D.; Wan, S. *J. Chem. Soc., Dalton Trans.* **1996**, 1323 and references therein.
(20) Scott, P.; Hitchcock, P. B. *J. Organomet. Chem.* **1995**, *497*, C1.

S0276-7333(96)00405-0 CCC: $12.00

Experimental Section

Reagents and General Techniques. All manipulations were carried out by using standard Schlenk, vacuum-line, and syringe techniques under an atmosphere of oxygen-free Ar. All the solvents for synthetic use were reagent grade. 1,2-Dimethoxyethane (DME), hexane, and tetrahydrofuran (THF) were dried and distilled over sodium in the presence of benzophenone ketyl under an Ar atmosphere, CH_2Cl_2 was dried and distilled over CaH_2 under an Ar atmosphere, acetone was dried and distilled over $CaCl_2$ under an Ar atmosphere, and propylene carbonate (PC) was stored over molecular sieves (5 Å) under an Ar atmosphere. All the solvents were bubbled with Ar for 1 h after distillation and stored under Ar or degassed by means of at least 3 freeze−pump−thaw cycles after distillation and before use. Column chromatography was performed by using Alfa neutral alumina at activity II. The compounds Na(η^5-$C_5H_4CO_2Me$) and $FvMo_2(CO)_6$ (**5**) were prepared according to literature procedures,[10a,21] and all reagents were used without further purification unless otherwise noted. The molybdenum content in compound **4** was separated with α-benzoinoxime and determined as the oxide.[22] The mercury content in **4** was determined by cold vapor atomic absorption spectrometry at 253.7 nm, using the standard procedure (Perkin-Elmer: *Analytical Methods for Atomic Absorption Spectrometry*). The ^{1}H and ^{199}Hg NMR spectra were recorded on a Bruker AMX-300 instrument. Chemical shifts were measured relative either to an internal reference of tetramethylsilane or to residual protons of the solvents for ^{1}H and neat dimethylmercury for ^{199}Hg. Infrared spectra were measured on a Perkin-Elmer 1650 infrared spectrometer. Elemental analyses were performed by the Mycroanalytical Laboratory of the University Autónoma of Madrid on a Perkin-Elmer 240 B microanalyzer. Electronic spectra were recorded on a Pye Unicam SP 8-100 UV−visible spectrophotometer. Mass spectra were measured on a VG-Autospec mass spectrometer for FAB or AIE by the Mass Laboratory of the University Autónoma of Madrid. A Perkin-Elmer Model 372 atomic absorption spectrophotometer equipped with the mercury analysis system was used for the analysis of mercury.

Preparation of a Dicarbomethoxydihydrofulvalene Solution. In an inert atmosphere, a 500 mL two-neck round bottom flask was equipped with a magnetic stirred bar and charged with Na(η^5-$C_5H_4CO_2Me$) (4.38 g, 30 mmol). The flask was sealed with rubber septa, and dry, oxygen-free THF (100 mL) was added via cannula. The resulting stirred solution was then cooled to −78 °C. Iodine (3.81 g, 15.0 mmol) in dry degassed THF (25 mL) was added by syringe. The flask was allowed to warm until room temperature (with stirring) for exactly 25 min, and chilled (0 °C) degassed hexane (150 mL) and cold aqueous 1% $Na_2S_2O_3$ (100 mL) were added. The two-phase mixture was shaken vigorously for 30 s, allowed to separate and then quickly cooled to −78 °C. This caused the aqueous layer to freeze, and the hexane layer was then decanted via cannula into a cold (−78 °C) Ar-filled, 1-L flask containing Na_2SO_4 (50 g). The clear orange dicarbomethoxydihydrofulvalene solution was decanted via cannula into a cold (−78 °C) Ar-filled, 1-L flask. The resulting solution was stored under Ar at this temperature until use.

Preparation of (η^5:η^5-$(C_5H_3CO_2Me)_2$)$Mo_2(CO)_6$. Separation of Two Isomers. A solution of $Mo(CO)_6$ (5.27 g, 20.0 mmol) in dry degassed glyme (400 mL) was heated to reflux under Ar. Without delay the dicarbomethoxydihydrofulvalene solution was added via syringe in 5-mL aliquots over a period of 4 h and the mixture refluxed for an additional 89 h. After being cooled, the entire reaction mixture was filtered through a CH_2Cl_2-packed alumina column (200 g). The column was washed with CH_2Cl_2 and the total eluent concentrated to about 40 mL causing the precipitation of $Mo(CO)_6$, which was filtered out. The solution was concentrated to give a purple powder; in the ^{1}H NMR spectrum of this solid six signals appeared in the range 6.09−4.28 ppm owing to the Fv ligand. The solid was redissolved in CH_2Cl_2 and purified by thin-layer chromatography (TLC) using CH_2Cl_2/hexane (1:1) as eluent to yield the purple isomers **1** (130 mg, 2.2%) and **2** (470 mg, 7.8%) as the major products. **1**: ^{1}H NMR (300 MHz, $CDCl_3$) δ 6.09 (dd, 2H, 8,8′ protons, $J_{8,4}$ = 2.90 Hz), 4.94 (t, 2H, 4,4′ protons, $J_{8,5}$ = 3.15 Hz), 4.68 (dd, 2H, 5,5′ protons, $J_{4,5}$ = 3.33 Hz), 3.74 (s, CO_2Me). Anal. Calcd for $C_{20}H_{12}O_{10}Mo_2$: C, 39.76; H, 1.99. Found: C, 39.63; H, 2.09. **2**: ^{1}H NMR (300 MHz, $CDCl_3$) δ 5.89 (d,d, 2H), 5.17 (t, 2H), 4.28 (d,d, 2H), 3.55 (s, CO_2Me). Anal. Found: C, 39.58; H, 2.12.

Preparation of Li_2[(η^5:η^5-$(C_5H_3CO_2Me)_2$)$Mo_2(CO)_6$] (3). A 1 M solution of lithium triethylborohydride in THF (2.5 mL, 2.5 mmol) was added dropwise to a solution of **2** (0.47 g, 0.77 mmol) in THF (40 mL) at 0 °C. During the addition period the solution gradually changed from purple to yellow. Et_3B was removed under high vacuum along with the solvent and gave **3** as a yellow, air-sensitive powder in quantitative yield. ^{1}H NMR (300 MHz, $CDCl_3$): δ 5.58 (m, 4H, Fv protons), 4.87 (dd, 2H, Fv), 3.66 (s, CO_2Me).

Preparation of (η^5:η^5-$(C_5H_3CO_2Me)_2$)$Mo_2(CO)_6Hg$ (4). A solution of **3** in fresh THF (15 mL) at room temperature was poured into 40 mL of an aqueous solution of 0.4 g (1.58 mmol) of mercury(II) cyanide. A yellow precipitate of the mercury derivative was formed. This was filtered off, washed several times with water, and dried in vacuum. Purification by TLC (acetone/hexane (1:1)) gave the brownish-yellow compound **4** as the major product. Yield: 300 mg (48%). ^{1}H NMR (300 MHz, $CDCl_3$): δ 5.90 (dd, 2H, 8,8′ protons, $J_{8,4}$ = 2.90 Hz), 5.17 (t, 2H, 4,4′ protons, $J_{8,5}$ = 3.15 Hz), 4.29 (dd, 2H, 5,5′ protons, $J_{4,5}$ = 3.33 Hz), 3.55 (s, CO_2Me). ^{199}Hg NMR (300 MHz, acetone-d_6): δ 301 (s). Anal. Calcd for $C_{20}H_{12}O_{10}Mo_2Hg$: Mo 23.84; Hg, 24.92. Found: Mo, 23.98; Hg, 24.59. MS: m/e 607 (M^+ − Hg), 340 (−CO), 312 (−2CO), 284 (−3CO), 248 (C_5H_4Mo).

X-ray Crystallography. Purple, prismatic crystals of 1,1′-(η^5:η^5-$(C_5H_3CO_2Me)_2$)$Mo_2(CO)_6$, **1**, are obtained from slow evaporation of a 1:10 dichloromethane−hexane solution of the complex. Dark blue, block-shaped crystals of isomer **2** are also obtained from slow evaporation of a 1:10 dichloromethane−hexane solution of the complex. Intensity data were collected on a Siemens P4 diffractometer using graphite-monochromated Mo Kα radiation. The unit cell dimensions were determined and refined using the positions of 18 high-angle reflections ($19.5° < 2\theta < 42°$) for **1** and 39 reflections ($16° < 2\theta < 32°$) for **2**. The intensities of three standard reflections measured every 97 reflections showed no decay during data collection for both structures. Lorentz, polarization, and background corrections were applied to the data using the Siemens P4 software.

Isomer 1. The systematic absences, *hkl* for $h + k$ odd and *h0l* for *l* odd, are consistent with either space groups *Cc* or *C*2/*c*. The intensity data provided strong evidence for the centric space group *C*2/*c*. The structure was successfully solved and refined in space group *C*2/*c*. The position of Mo atom was solved by the Patterson method, and the remaining non-H atoms were located by successive difference Fourier syntheses. Non-hydrogen atoms were refined anisotropically, and hydrogen atoms were refined isotropically by full matrix least-squares on F^2. The three H atoms on the cyclopentadienyl ring, H(4a), H(5a), and H(6a), refined to C−H distances of 0.87(5), 0.74(7), and 0.87(7) Å, respectively. The methyl H atoms were refined as a tetrahedral group varying the C−H distance, which refined to a value of 0.86(5) Å. No secondary extinction correction was applied to the data. All calculations were perfomed using the SHELXTL PC version[23] on a 486 personal computer.

(21) Hart, W. P.; Shihua, D.; Rausch, M. D. *J. Organomet. Chem.* **1985**, *282*, 111.

(22) Furman, N. H. *The Elements*; Vol. 1 of *Standard Methods of Chemical Analysis*, 6th ed.; D. Van Nostrand Co., Inc., Princeton, NJ; p 675.

(23) Sheldrick, G. M. *SHELXTL/PC, Users Manual*; Siemens Analytical X-ray Instruments Inc.: Madison, WI, 1990.

Table 1. Crystal Data and Structure Refinements

	compd	
	1	**2**
empirical formula	$C_{20}H_{12}Mo_2O_{10}$	$C_{20}H_{12}Mo_2O_{10}$
fw	604.18	604.18
temp (K)	293(2)	173(2)
wavelength (Å)	0.710 73	0.710 73
cryst system	monoclinic	monoclinic
unit cell dimens (Å, deg)	$a = 13.787(3)$	$a = 14.551(1)$
	$b = 16.889(2)$	$b = 11.336(1)$
	$c = 9.854(1)$	$a = 12.220(2)$
	$\beta = 110.45(1)$	$\beta = 93.30(1)$
V, (Å^3), Z	2149.9(6), 4	2012.3(4), 4
D (calcd) (Mg/m^3)	1.867	1.994
abs coeff (mm^{-1})	1.221	1.304
F(000)	1184	1184
cryst size (mm)	0.30 × 0.18 × 0.20	0.48 × 0.40 × 0.32
θ range for data collcn (deg)	2.41−25.02	2.78−30.02
limiting indices	$-1 \le h \le 16$, $-1 \le k \le 20$, $-11 \le l \le 11$	$-20 \le h \le 20$, $-15 \le k \le 0$, $0 \le l \le 17$
reflcns collcd	2321	6110
indepdt reflcns	1906 ($R_{int} = 0.0452$)	5857 ($R_{int} = 0.0138$)
abs corr	semi-empirical from ψ-scans	SHELXA
max and min transm	0.809 and 0.606	0.907 and 0.660
refinement method	full-matrix least squares on F^2	full-matrix least squares on F^2
data/restraints/parameters	1906/0/160	5857/0/318
goodness-of-fit on F^2	1.089	1.124
final R indices ($I > 2\sigma(I)$)	$R1 = 0.0513$, w$R2 = 0.0905$	$R1 = 0.0231$, w$R2 = 0.0612$
R indices (all data)	R1 = 0.1056, wR2 = 0.1119	R1 = 0.0265, wR2 = 0.0623
largest diff peak and hole (e Å^{-3})	0.482 and −0.949	0.391 and −0.807

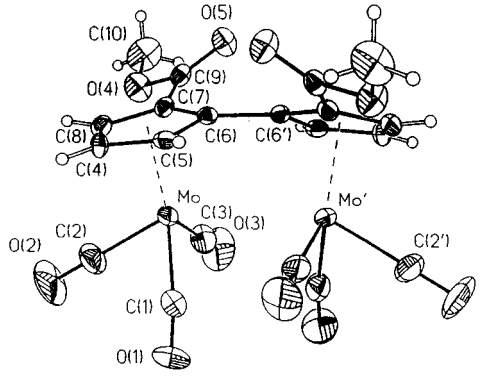

Figure 1. View of molecule **1** with 25% probability ellipsoids drawn for Mo, C, and O. For clarity, H atoms are represented as open spheres.

Isomer 2. The systematic absences, *0k0* for *k* odd and *h0l* for *l* odd, are only consistent with the space group $P2_1/c$. The position of Mo atom was solved by the Patterson method, and the other non-H atoms were located by successive difference Fourier syntheses. Non-hydrogen atoms were refined anisotropically and hydrogen atoms were refined isotropically by full-matrix least squares on F^2. The three H atoms on the cyclopentadienyl rings, H(4a), H(5a), and H(8a) and H(14a), H(15a), and H(18a), refined to C−H distances of 0.98(3), 0.95(2), and 0.96(3) and 0.95(3), 0.97(2), and 0.90(3) Å, respectively. The methyl H atoms were refined as a tetrahedral group varying the C−H distance, which refined to values of 0.93(2) Å for C(10) and 0.96(2) Å for C(20). No secondary extinction correction was applied to the data.

Selected experimental details of the X-ray determination are given in Table 1. Final positional parameters, anisotropic thermal parameters, and hydrogen atom parameters are available as Supporting Information. Tables 2 and 3 contain selected bond distances and angles. Figures 1 and 2 present molecular diagrams of **1** and **2**, respectively.

Electrochemical Measurements. A PAR Model 273 electrochemistry system and a 7047 A Hewlett Packard X-Y recorder were used. Positive feedback *iR* compensation was employed in order to minimize the effects of solution resistance. All experiments were carried out in a three-electrode cell under N_2 atmosphere in anhydrous deoxygenated solvent. Temperature was maintained constant at 25 °C. Solutions contained 0.2 M tetrabutylammonium hexafluorophosphate (TBA(PF_6)) as supporting electrolyte and either THF or PC as solvent.

Cyclic voltammetry studies were made on a pc-Pt working electrode (0.05 cm^2 real surface area, as calculated in a separate experiment through the H-adatom charge in 0.5 M H_2SO_4 solution[24]). The counter electrode was Pt gauze. The reference electrode was an Ag wire quasi-reference electrode (QRE); the silver wire was pretreated by immersion in 10 M HNO_3 for 5 min before use. After a series of experiments, the QRE potential was calibrated by adding ferrocene (Fc) to the solution and taking voltammograms of the ferrocenium/ferrocene system. Potentials in this paper are then referred to this couple, Fc^+/Fc, which has been recommended as a standard reference in nonaqueous solvents.[25] It can be related

Table 2. Selected Bond Lengths (Å) and Angles (deg) for 1

Bond Lengths			
Mo−C(2)	1.970(10)	Mo−C(3)	1.978(11)
Mo−C(1)	1.985(11)	Mo−C(5)	2.318(8)
Mo−C(8)	2.318(8)	Mo−C(6)	2.320(6)
Mo−C(4)	2.337(7)	Mo−C(7)	2.346(7)
O(1)−C(1)	1.135(12)	O(2)−C(2)	1.135(11)
O(3)−C(3)	1.131(11)	O(4)−C(9)	1.317(9)
O(4)−C(10)	1.471(11)	O(5)−C(9)	1.196(9)
C(4)−C(5)	1.373(11)	C(4)−C(8)	1.410(11)
C(5)−C(6)	1.436(10)	C(6)−C(7)	1.434(10)
C(6)−C(6)[a]	1.474(12)	C(7)−C(8)	1.398(10)
C(7)−C(9)	1.482(11)		
Angles			
C(2)−Mo−C(3)	80.5(4)	C(2)−Mo−C(1)	79.8(5)
C(3)−Mo−C(1)	100.1(5)	C(9)-O(4)−C(10)	115.3(7)
O(1)−C(1)−Mo	174.0(9)	O(2)−C(2)−Mo	177.8(11)
O(3)−C(3)−Mo	175.1(10)	C(5)−C(4)−C(8)	108.5(7)
C(4)−C(5)−C(6)	108.5(8)	C(7)−C(6)−C(5)	106.8(6)
C(7)−C(6)−C(6)[a]	126.4(8)	C(5)−C(6)−C(6)[a]	125.7(8)
C(8)−C(7)−C(6)	107.0(7)	C(8)−C(7)−C(9)	125.4(7)
C(6)−C(7)−C(9)	126.9(6)	C(7)−C(8)−C(4)	109.2(7)
O(5)−C(9)-O(4)	125.5(8)	O(5)−C(9)−C(7)	124.6(7)
O(4)−C(9)−C(7)	109.9(7)		

[a] Symmetry transformation used to generate equivalent atoms: $-x, y, -z + 1/2$.

(24) Woods, R. In *Electroanalytical Chemistry*; Bard, A. J., Ed.; Academic: New York, 1976; Vol. 9.

Table 3. Selected Bond Lengths (Å) and Angles (deg) for 2

Bond Lengths

Mo(1)−C(3)	1.984(2)	Mo(1)−C(2)	1.986(2)	Mo(1)−C(1)	1.992(2)
Mo(1)−C(6)	2.323(2)	Mo(1)−C(5)	2.324(2)	Mo(1)−C(8)	2.335(2)
Mo(1)−C(4)	2.353(2)	Mo(1)−C(7)	2.369(2)	Mo(2)−C(11)	1.984(2)
Mo(2)−C(12)	1.990(2)	Mo(2)−C(13)	2.010(2)	Mo(2)−C(17)	2.326(2)
Mo(2)−C(16)	2.328(2)	Mo(2)−C(18)	2.339(2)	Mo(2)−C(15)	2.344(2)
Mo(2)−C(14)	2.351(2)	O(1)−C(1)	1.148(2)	O(2)−C(2)	1.141(3)
O(3)−C(3)	1.147(3)	O(4)−C(9)	1.334(3)	O(4)−C(10)	1.442(3)
O(5)−C(9)	1.202(3)	O(11)−C(11)	1.147(2)	O(12)−C(12)	1.138(3)
O(13)−C(13)	1.141(3)	O(14)−C(19)	1.335(2)	O(14)−C(20)	1.453(3)
O(15)−C(19)	1.204(2)	C(4)−C(5)	1.410(3)	C(4)−C(8)	1.423(3)
C(5)−C(6)	1.463(3)	C(6)−C(7)	1.432(3)	C(6)−C(16)	1.465(3)
C(7)−C(8)	1.417(3)	C(7)−C(9)	1.487(3)	C(14)−C(15)	1.403(3)
C(14)−C(18)	1.423(3)	C(15)−C(16)	1.432(3)	C(16)−C(17)	1.465(3)
C(17)−C(18)	1.417(3)	C(17)−C(19)	1.484(3)		

Angles

C(3)−Mo(1)−C(2)	81.61(9)	C(3)−Mo(1)−C(1)	97.10(8)	C(2)−Mo(1)−C(1)	79.48(8)
C(3)−Mo(1)−C(6)	109.79(7)	C(1)−Mo(1)−C(5)	104.53(8)	C(6)−Mo(1)−C(5)	36.72(6)
C(2)−Mo(1)−C(8)	84.27(8)	C(5)−Mo(1)−C(4)	35.09(7)	C(6)−Mo(1)−C(7)	35.52(7)
C(8)−Mo(1)−C(7)	35.04(7)	C(11)−Mo(2)−C(12)	80.50(9)	C(11)−Mo(2)−C(13)	99.17(8)
C(12)−Mo(2)−C(13)	80.86(9)	C(13)−Mo(2)−C(17)	106.22(7)	C(11)−Mo(2)−C(16)	108.72(8)
C(17)−Mo(2)−C(16)	36.69(6)	C(17)−Mo(2)−C(18)	35.37(7)	C(16)−Mo(2)−C(15)	35.68(7)
C(15)−Mo(2)−C(14)	34.79(7)	C(9)-O(4)−C(10)	114.7(2)	C(19)-O(14)−C(20)	114.8(2)
O(1)−C(1)−Mo(1)	175.5(2)	O(2)−C(2)−Mo(1)	179.2(2)	O(3)−C(3)−Mo(1)	177.1(2)
C(5)−C(4)−C(8)	107.6(2)	C(5)−C(4)−Mo(1)	71.32(11)	C(4)−C(5)−C(6)	108.4(2)
C(4)−C(5)−Mo(1)	73.59(12)	C(6)−C(5)−Mo(1)	71.60(11)	C(7)−C(6)−C(5)	106.6(2)
C(7)−C(6)−C(16)	131.8(2)	C(5)−C(6)−C(16)	120.7(2)	C(7)−C(6)−Mo(1)	74.02(11)
C(16)−C(6)−Mo(1)	111.22(12)	C(8)−C(7)−C(6)	107.8(2)	C(8)−C(7)−C(9)	120.5(2)
C(6)−C(7)−C(9)	130.7(2)	C(8)−C(7)−Mo(1)	71.15(11)	C(9)−C(7)−Mo(1)	132.62(14)
C(7)−C(8)−C(4)	109.5(2)	C(7)−C(8)−Mo(1)	73.80(11)	O(5)−C(9)-O(4)	125.6(2)
O(5)−C(9)−C(7)	124.2(2)	O(4)−C(9)−C(7)	109.8(2)	O(11)−C(11)−Mo(2)	174.6(2)
O(12)−C(12)−Mo(2)	177.1(2)	O(13)−C(13)−Mo(2)	176.1(2)	C(15)−C(14)−C(18)	108.1(2)
C(15)−C(14)−Mo(2)	72.34(11)	C(14)−C(15)−C(16)	109.3(2)	C(14)−C(15)−Mo(2)	72.88(12)
C(15)−C(16)−C(17)	106.4(2)	C(15)−C(16)−C(6)	120.1(2)	C(17)−C(16)−C(6)	132.0(2)
C(15)−C(16)−Mo(2)	72.75(11)	C(6)−C(16)−Mo(2)	110.25(12)	C(18)−C(17)−C(16)	107.2(2)
C(18)−C(17)−C(19)	122.7(2)	C(16)−C(17)−C(19)	130.2(2)	C(18)−C(17)−Mo(2)	72.81(11)
C(19)−C(17)−Mo(2)	120.26(13)	C(17)−C(18)−C(14)	109.0(2)	C(17)−C(18)−Mo(2)	71.82(11)
O(15)−C(19)-O(14)	123.7(2)	O(15)−C(19)−C(17)	125.8(2)	O(14)−C(19)−C(17)	110.5(2)

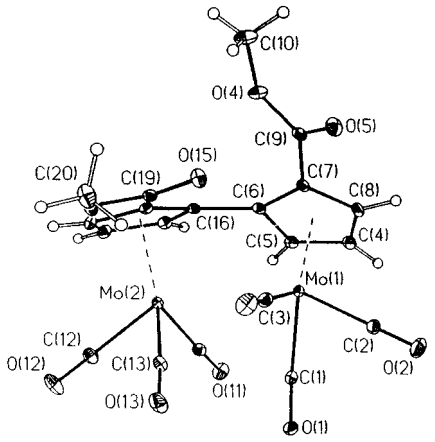

Figure 2. View of molecule **2** with 25% probability ellipsoids drawn for Mo, C, and O. For clarity, H atoms are represented as open spheres.

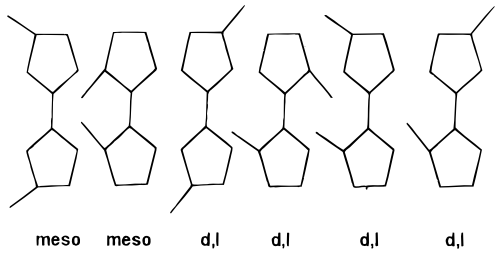

Figure 3. Schematic representation of the six possible isomers, not including enantiomers, of (η^5:η^5-$(C_5H_3CO_2Me)_2$)$Mo_2(CO)_6$.

to a SCE reference electrode by using a value of +0.307 V vs SCE for Fc^+/Fc.[26]

Controlled-potential coulometry studies were made on a large area pc-Pt working electrode. The other electrodes were the same as in cyclic voltammetry, although special care was taken in order to place the counterelectrode in a separate compartment avoiding diffusion of electroactive species.

Results and Discussion

Synthesis and Spectroscopic Properties. Following the procedure described by Vollhardt for the synthesis of a dihydrofulvalene solution,[27] we have prepared a dicarbomethoxydihydrofulvalene solution. By reaction between this solution and $Mo(CO)_6$, the complex (η^5:η^5-$(C_5H_3CO_2Me)_2$)$Mo_2(CO)_6$ has been obtained. Of the six possible steroisomers (Figure 3), we have obtained and separated by TLC only two, in a very low yield. The reaction of **2** with $LiEt_3BH$ in THF leads to the dianion salt $\mathbf{2}^{2-}(Li^+)_2$ (**3**), which reacts with an aqueous solution of $Hg(CN)_2$ giving rise to (η^5:η^5-$(C_5H_3CO_2Me)_2$)$Mo_2(CO)_6Hg$ (**4**).

The IR spectra of **1**, **2**, and **4** exhibit five absorption bands in the range 2100−1700 cm^{-1}: four of them are associated with terminal Mo−CO stretching (ν_{CO}) modes and the fifth with ν_{CO} of the CO_2Me group (Table 4). The Mo−CO stretching modes appear at higher frequencies than the corresponding band when R = H, and this is due to the electron-withdrawing properties of the carbomethoxy substituent in the Fv ring, making Mo

(25) Gritzner, G.; Kuta, J. *Pure Appl. Chem*. **1982**, *54*, 1527.
(26) Bard, A. J.; Faulkner, L. R. *Electrochemical Methods*; Wiley: New York, 1980.
(27) Vollhardt, K. P. C.; Weidman, T. W. *Organometallics* **1984**, *3*, 82.

Table 4. IR and UV−Vis Spectroscopic Data for the Complexes 1−5 (cm^{-1}, THF)

	IR		UV−vis (nm)	
compd	ν_{CO} (cm^{-1})	ν_{CO} (CO_2CH_3) (cm^{-1})		
1	2022.3 (vs), 1973.9 (vs), 1933.9 (s), 1925.6 (sh), 1897.2 (w)	1729.7 (m)	565	378
			565[b]	380[b]
2	2023.9 (vs), 1973.2 (vs), 1943.3 (s), 1923.1 (sh), 1899.7 (w)	1730.5 (m)	572	379
3	1902.1 (vs), 1804.0 (sh), 1796.9 (vs), 1792.4 (sh)	1736.2 (m)		
4	2023.7 (m), 1995.9 (s), 1971.3 (vs), 1902.7 (s, br)	1725.8 (s)		372
5	2010 (vs), 1960 (vs), 1925 (vs), 1905 (sh), 1880 (sh)[a]		555	378

[a] Reference 10a. [b] Data in PC.

Table 5. Comparison of Structural Data in 1, 2, and 5

	complex		
	1	**2**	**5**
Mo···Mo dist[a]	3.270(4)	3.238(1)	3.371(1)
Mo−Cp[a,b]	1.995(10)	2.000(2), 1.997(2)	1.990(1), 1.992(1)
C−C bridgehead[a]	1.474(12)[c]	1.465(3)[d]	1.442(2)[e]
av C═O dist[a]	1.134(1)	1.144(2)	1.147(3)
bend angle (dihedral angle betwn Cp rings) θ (deg)	32.2	32.3	15.3

[a] In angstroms, Å. [b] Refers to metal-to-Cp ring centroid distance. [c] Refers to C(6)−C(6′) distance in **1**. [d] Refers to C(6)−C(16) distance in **2**. [e] Refers to C(5)−C(6).[1]

less electron-rich, which reduces the back-bonding between Mo and CO. In **3** the infrared carbonyl stretching bands were observed at 1902, 1797, and 1792 cm^{-1}; these low-energy absorptions are typical of metal carbonyl anions in which there is strong electron back-donation from the metal to the carbonyl ligands.

The ^1H NMR spectra of **1**, **2**, and **4** show three Fv signals (ABX system) at δ 6.09, 4.94, and 4.68 (**1**), 5.89, 5.17, and 4.28 (**2**), and 5.90, 5.17, and 4.29 (**4**) and a singlet signal at 3.74, 3.55, and 3.55 for **1**, **2**, and **4**, respectively, arising from the methyl protons of CO_2-Me.

The ^{199}Hg NMR chemical shift of **4** is observed at 301 ppm. The ^1H NMR of (η^5:η^5-($C_5H_3CO_2Me$)$_2$)$Mo_2(CO)_6$-Hg is very similar to the Fv parent, and the ^{199}Hg NMR value lies in the region characteristic of complexes containing molybdenum−mercury bonds and substituted-cyclopentadienyl ligands.[28] The shift to downfield suggests that the mercurial compound is a relatively covalent, nonpolar system. This compound is the first example of a characterized mercurial Fv compound described in the literature, since the reaction of the (fulvalene)hexacarbonyldimolybdenum dianion with mercury acetate yielded a small amount of uncharacterized yellow material.[10a]

Description of the Crystal and Molecular Structures of 1 and 2. For both isomers **1** and **2**, the crystal structures consist of discrete molecules in the unit cell. Complex **1** has C_2 symmetry, with a crystallographic 2-fold axis bisecting the molecule. The 2-fold axis coincides with the line joining the midpoints of the symmetry-related atoms Mo/Mo′ and C(6)/C(6′). (Wyckoff *e*, site symmetry 2). Both **1** and **2** consist of two $Mo(CO)_3$ units which are bridged by a carbomethoxy-substituted Fv ligand as shown in Figures 1 and 2. The Fv ligands adopt the 1,1′-(η^5:η^5) binding mode, and the Mo centers have a piano stool structure. In isomer **1** the Fv ligands have $-CO_2Me$ groups *trans* with respect to the bridgehead C−C bond, while the groups are *cis* in isomer **2**.

The molecular shapes of **1** and **2** are similar to that of the unsubstituted analogue (η^5:η^5-C_5H_4)$_2Mo_2(CO)_6$, **5**.[1] Some structural differences among **1**, **2**, and **5** arise as a result of the presence of the $-CO_2Me$ groups in **1** and **2**, and these are listed in Table 5. The substituted Fv ligands in **1** and **2** are electron deficient when compared to that of the parent Fv in **5**. The presence of the electron-withdrawing $-CO_2Me$ groups on the Fv ligands reduces the Lewis basicity of the ligand. This results in the reduction of electron density at the Mo center in **1** and **2**. The reduced donicity of the Cp ligands in isomers **1** and **2** is offset by an increase in the metal−metal interaction. Thus the Mo···Mo distances in **1**, 3.270(4) Å, and **2**, 3.238(1) Å, are significantly shorter than that observed in **5**, 3.371(2) Å. Another structural parameter that reflects the extent of metal−metal interaction in complexes of this type is the value of the bend angle θ (the dihedral angle between the two Cp planes of the fulvalene ligand). In general θ increases with an increase in metal−metal interaction. Shortening of metal−metal distance forces the Fv ring to bend away from planarity. The values of θ in **1** and **2**, 32.2 and 32.3°, respectively, are greater than that observed in **5**, 15.3°. The shortening of the Mo−Mo distance in **1** also affects the C−C distance at the bridgehead linking the two Cp rings. The corresponding C−C distances in **1** (1.474(12) Å) and **2** (1.465(3) Å) are longer than that observed in **5** (1.428(2) Å), although the differences are barely significant.

The Mo−Cp ring carbon distances range 2.318(8)−2.346(7) Å in **1** and 2.323(2)−2.369(2) Å in **2**; these values are consistent with Mo−Cp ring carbon distances seen in other dimolybdenum compounds. The mean C═O bond lengths, 1.134(1) Å in **1**, 1.144(2) Å in **2**, and 1.147(3) Å in **5**, do not reflect a significant reduction in the Mo−CO π-back-bonding in **1** and **2**, as suggested by the solution IR spectral studies. All other distances and angles are normal.[29]

Electrochemical Studies. Reduction of 1 and 2. Reduction of **1** involves a cathodic wave to form a reduced species that is oxidized on a subsequent anodic scan at a much more positive potential (Figure 4). The potentials at which these processes take place depend on the solvent (Table 6). The overall number of electrons transferred was determined by controlled-poten-

(28) Kubicki, M. M.; Le Gall, J. Y.; Pichon, R.; Salaum, J. Y.; Cano, M.; Campo, J. A. *J. Organomet. Chem.* **1988**, *348*, 349 and references therein.

(29) Allen, F. H.; Kennard, O. *Chem. Design Automation News* **1993**, *8*, 31.

Table 6. Electrochemical Data for 1

	redn $\mathbf{1} \rightarrow \mathbf{1}^{2-}$		reoxidn $\mathbf{1}^{2-} \rightarrow \mathbf{1}$		oxidn $\mathbf{1} \rightarrow \mathbf{1}^{2+}$	
	THF	PC	THF	PC	THF	PC
E_p (V vs Fc^+/Fc)[a]	−1.37	−1.20	−0.70	−0.39	+0.75	+0.65
i_p/C (mA cm^{-2} M^{-1})	320	110	150	60	ca. 360	160
E_p vs log v slope (mV)	65	95	81	75		45
α (from E_p vs log v)	0.46	0.32	0.37[b]	0.40[b]		0.67[b]
$\lvert E_p - E_{p/2}\rvert$ (mV)	105	125				70
α (from $\lvert E_p - E_{p/2}\rvert$)	0.45	0.38				0.68[b]

[a] Data obtained at $v = 0.1$ V s^{-1}. [b] 1 − α.

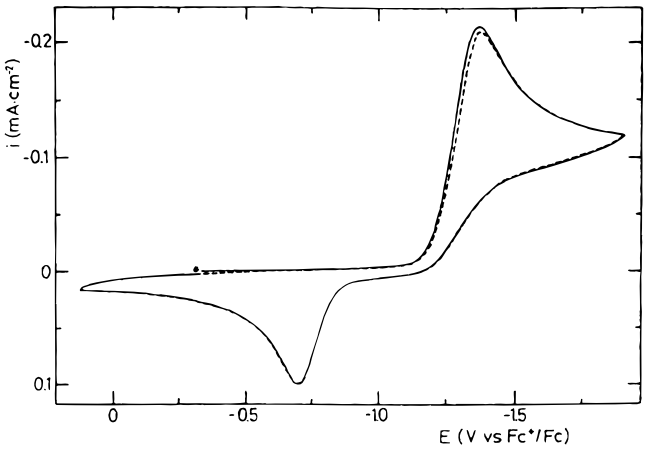

Figure 4. Cyclic voltammogram for the reduction of a 6.7 × 10^{-4} M solution of **1** in THF containing 0.2 M $TBAPF_6$ at 0.1 V s^{-1} and 25 °C. The first (—) and second (- - -) scans are shown. An asterisk indicates the start of a cycle.

tial coulometry. Thus, a weighted amount of compound was dissolved in 0.2 M TBA(PF_6) in PC (yielding a purple solution) and reduced at −1.5 V vs Fc^+/Fc, a potential well within the diffusion-limited region of the reduction wave. The amount of electricity consumed when the current decayed to background (after ca. 1 h and 30 min) and the color of the solution as pale yellow indicated that the reduction was a two-electron process.

Coulometrical oxidation of the reduced product was also attempted. However, the solution never turned back to the original purple colour; after ca. 1 h and 30 min with the consumption of less than 2 F/mol, the solution was brownish-pink and a cyclic voltammogram showed the presence of peaks that did not appear in the original one and were difficult to identify. Thus, probably some decomposition had taken place.

An analysis of the reduction and reoxidation peaks at different scan rates reveals that i_{pc} and i_{pa} depend linearly on the square root of the scan rate in the range 0.01 V $s^{-1} < v < 1$ V s^{-1}. A systematic shift in the peak potentials with scan rates was observed for both processes. The plot of E_p vs log v is linear for v up to 1 V s^{-1}. The slopes of these plots are assembled in Table 6.

The width of the wave was also studied. Experimentally observed $\lvert E_p - E_{p/2}\rvert$ values, where $E_{p/2}$ is the potential at half-height, are also shown in Table 6 for the reduction process. Although dependent on the solvent, they are always greater than 30 mV, the value which would correspond to a reversible, diffusion-controlled, two-electron transfer.

The linear dependance of E_p with log v, with slopes greater than 60 mV per decade, so as the width of the wave, are indicative of irreversible charge transfer. The transfer coefficient, α, can be calculated from the E_p vs log v plot according to the following equation:[30]

$$E_p = (2.3RT/2\alpha n_\alpha F) \log v + \text{constant} \qquad (1)$$

Here n_α is the number of electrons transferred in the rate-limiting step. Calculated α values (1 − α for reoxidation) assuming $n_\alpha = 1$ are assembled in Table 6. Alternatively, α can be calculated from the width of the wave according to[30]

$$\lvert E_p - E_{p/2}\rvert = 1.857\,(RT/\alpha n_\alpha F) \qquad (2)$$

Table 6 also lists α values calculated by this method, which are consistent with those obtained from the E_p vs log v slope.

All the above data suggest that the reduction follows an ECE type mechanism, as has been found for related compound $[Mo(CO)_3Cp]_2$[31] or the fulvalene complex $FvMo_2(CO)_6$.[32] A first electron is added to a metal−metal antibonding orbital (σ*). This rate-determining electron transfer is followed by the relaxation of the molecule geometry through an increase in the metal−metal distance. The latter is a fast homogeneous chemical reaction which yields an anion radical in a less strained geometry and a decrease in the σ−σ* energy gap. Now, the reduction of the anion radical takes place more easily than for the starting compound; that is, it is readily electroreducible at the reduction potential of **1**. Therefore, an overall two-electron transfer is observed, yielding the dianion $\mathbf{1}^{2-}$, in which there is no Mo−Mo bond.

Reoxidation of $\mathbf{1}^{2-}$ is consistent with an ECE mechanism. A first electron is removed from an orbital localized at one of the Mo centers. A following chemical step leads to the formation of a partial Mo−Mo bond in the $\mathbf{1}^-$ anion radical, which readily loses another electron from the σ* antibonding orbital, regenerating **1**.

In order to confirm the reduction mechanism, cyclic voltammetry of $Li_2[(\eta^5:\eta^5\text{-}(C_5H_3CO_2Me)_2)Mo_2(CO)_6]$ (**3**) (the lithium salt of the dianion $\mathbf{1}^{2-}$) was carried out in THF. A first scan starting at −1.0 V shows an oxidation peak at −0.70 V. This value is coincident with that found for the reoxidation of the reduction product of **1** and corroborates the proposed mechanism.

Changing the solvent involves different values of E_{pc}. The observed trend is also in accordance with the anion $\mathbf{1}^{2-}$ as the final product in the ECE reduction process, as well as with the presence of a negatively charged intermediate. Thus, in PC (solvent with a high dipole moment, 4.94 D) $E_{pc} = -1.20$ V, while in THF $E_{pc} = -1.37$ V. The presence of the polar molecules of PC

(30) Nicholson, R. S.; Shain, I. *Anal. Chem.* **1964**, *36*, 706.
(31) Kadish, K. M.; Lacombe, D. A.; Anderson, J. E. *Inorg. Chem.* **1986**, *25*, 2246.
(32) Moulton, R.; Weidman, T. W.; Vollhardt, K. P. C.; Bard, A. J. *Inorg. Chem.* **1986**, *25*, 1846.

stabilizes both the monocharged radical intermediate and the divalent ion formed after total reduction. Also significantly, the reoxidation potential is located 0.31 V more positive in PC than in THF, instead of the 0.17 V shift in the reduction process. The excess energy to be applied in order to oxidize the anion confirms the Marcus theory for charge transfer, since the activation energy for charge transfer is a function of the reorganization energy of the solvation layer. Thus, as the doubly reduced compound would give rise to a high orientation effect on the surrounding polar PC molecules, the value of λ, the reorganization energy of the solvation sphere, would consequently grow, the higher the dipole moment of the solvent. Therefore, for charge transfer to be achieved, an excess energy should be supplied, consistent with the location of the reoxidation of the reduced compound at a more positive potential. Thus, the 0.14 V more positive than expected value constitutes an indirect evaluation of the extra stabilizing energy induced by the polarity of the PC molecules ($\Delta\lambda$ = 13.5 kJ mol^{-1}).

Diffusion coefficients, D, of **1** were obtained from the chronoamperometric $i-t$ transient according to[33]

$$it^{1/2} = nFAC(D/\pi)^{1/2} \qquad (3)$$

where A is the electrode area and C is the bulk concentration of electroactive species. In THF, $D = 7.0 \times 10^{-6}$ cm^2 s^{-1}, whereas, in PC, a much more viscous solvent, $D = 1.1 \times 10^{-6}$ cm^2 s^{-1}. Values in both media agreed reasonably well with those expected from the direct application of the equation[26]

$$i_p = (2.99 \times 10^5)n(\alpha n_\alpha)^{1/2}ACD^{1/2}v^{1/2} \qquad (4)$$

which is valid for irreversible processes. Considering $n_\alpha\alpha = 0.45$ in THF and $n_\alpha\alpha = 0.35$ in PC, and averaging for results in the 0.01 V s^{-1} < v < 1 V s^{-1} range, eq 4 yields $D = 6.6 \times 10^{-6}$ cm^2 s^{-1} in THF and $D = 1.1 \times 10^{-6}$ cm^2 s^{-1} in PC.

The change in D when the solvent is PC or THF is that expected if the different viscosities (2.53 cP for PC and 0.46 cP for THF) are taken into account and Walden's rule[34] is applied.

In order to study the influence of the CO_2Me substituent on the values of E_{pc} and E_{pa}, an electrochemical investigation of the unsubstituted Fv complex $FvMo_2(CO)_6$, **5**, was carried out. Electrochemical results of **5** had previously been reported by Moulton et al.[32] However, there are some difficulties when trying to compare values in different solvents and somewhat different experimental conditions. In the present study, E_{pc} for the reduction of **5** was found at −1.52 V vs Fc^+/Fc in THF, whereas E_{pa} for the reoxidation takes place at −0.79 V. A significant positive shift in E_{pc} is observed from **5** to **1**. As already discussed, the substituent CO_2Me exerts an electron-withdrawing effect, which refers in an easier reduction of **1** as compared to **5**. Thus, E_{pc} is less negative for **1**, as observed.

Electrochemical reduction of **2** was also studied. Peaks and parameters were identical (within experimental error) to those found for **1** and assembled in Table 6. Therefore, we assume that the different space location of the substituents does not affect this process, which involves primarily metal-centered orbitals.

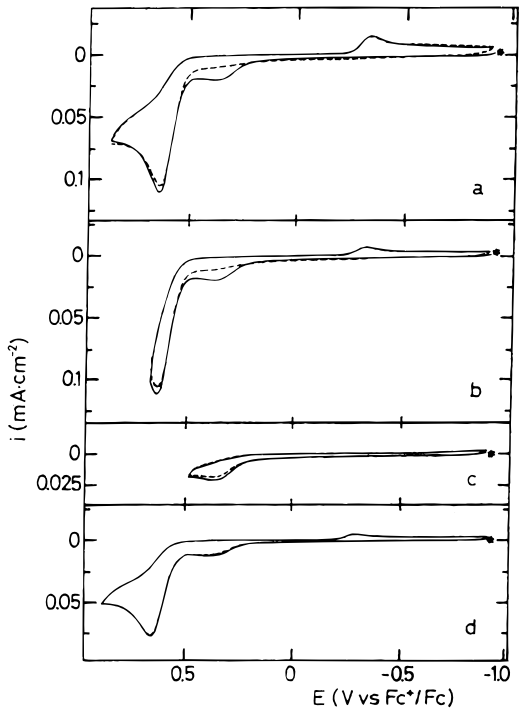

Figure 5. Cyclic voltammogram for the oxidation of a 6 × 10^{-4} M solution of **1** in PC containing 0.2 M TBA(PF_6) at 25 °C. The first (—) and second (- - -) scans are shown. An asterisk indicates the start of a cycle. The sweep rate is 0.1 V s^{-1} in a−c, and 0.05 V s^{-1} in d.

Oxidation of 1 and 2. The electrochemical oxidation of **1** is best studied in PC, a solvent with a larger anodic potential window than THF. The voltammogram shows an irreversible wave at +0.65 V (Figure 5, Table 6). This main wave is preceded by a prewave at ca. +0.35 V which disappears in the second and subsequent cycles provided the sweep is reversed beyond +0.6 V and the sweep rate is 0.1 V s^{-1} or faster. However, when the sweep rate is slower than 0.1 V s^{-1}, the second cycle is identical to the first one (Figure 5c). A very similar prewave was also found by Moulton et al.[32] for the related compound $FvMo_2(CO)_6$. They interpreted it as due to the formation of an adsorption species on the electrode. It seems a reasonable explanation for this case too, although we found that the integrated charge under the prewave was substantially smaller than that due to monolayer coverage.

Coulometry of the oxidation wave was attempted in PC, but results were not conclusive. Potential was set at +0.9 V and coulometry performed for 1 h and 30 min. The charge transferred was then less than 1 F/mol (ca. 0.7), and the solution acquired a brownish color. This result could be indicative of a one-electron process for the oxidation. However, a comparison of the peak height with that of the reduction process renders as very improbable that less than two electrons per molecule are transferred in the oxidation process. Furthermore, if a fresh Pt electrode is inmersed in the electrolyzed solution, the voltammogram shows the characteristic waves of **1**, indicating that a considerable amount of this product remains in solution. Therefore, we think that the electrode is passivated during the oxidation process at 0.9 V. A similar result was found by Moulton et al.,[32] who observed a coating on the electrode when the potential was positive enough in a $FvMo_2(CO)_6$ solution.

(33) Adams, R. N. *Electrochemistry at Solid Electrodes*; Marcel Dekker: New York, 1969.
(34) Walden, P.; Ulich, H.; Busch, G. *Z. Phys. Chem.* **1926**, *123*, 429.

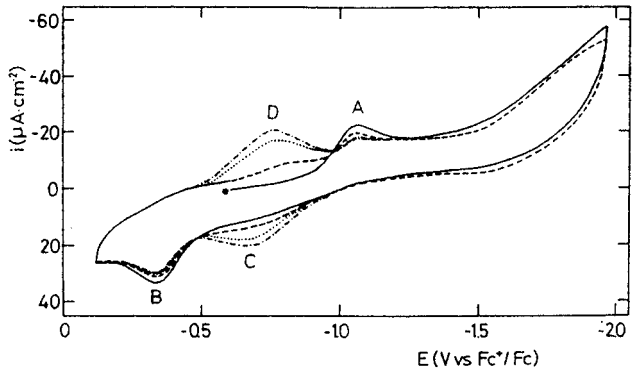

Figure 6. Cyclic voltammogram for the reduction of a 1.03 $\times$ 10^{-3} M solution of **4** in PC containing 0.2 M TBA(PF_6) at 0.1 V s^{-1} and 25 °C: (—) 1st, (- - -) 2nd, (···) 4th, and (- · -) 6th cycles. An asterisk indicates the start of measurement.

The oxidation wave is highly irreversible. However, on the return cathodic scan, a very small peak appears at ca. −0.32 V. This peak is unambigously associated with processes taking place in the main wave, as it does not appear when the anodic sweep is reversed just after the prewave and, on the contrary, it is shown in all the cycles when the sweep reversal takes place after the main wave (Figure 5).

The oxidation peak of **1** can be analyzed in a way similar to that carried out for the reduction peak. Thus, $1 - \alpha$ has been obtained from the E_p vs log v plot and from the width of the wave (Table 6).

E_p for the oxidation of **1** is significantly greater than for the unsubstituted $FvMo_2(CO)_6$, which we measured as +0.49 V in THF. As discussed by Moulton et al.,[32] the oxidation of these compounds must correspond to the removal of electrons from orbitals that are primarily ligand-localized, probably of the π_L type. The presence of the electron-withdrawing CO_2Me substituents in **1** stabilizes these π_L orbitals. Therefore, oxidation of **1** is more difficult. This is in accordance with the significantly more positive values of E_p(ox) observed.

Electrochemical oxidation of **2** was also studied. The shape and main features of the voltammograms are similar to those of **1**, i.e. an irreversible wave preceded by a prewave is obtained. However, E_p of the main wave is +0.56 V in PC, as compared to +0.65 V for **1**. As the only significant difference between both isomers is the space distribution of the CO_2Me substituents (*trans* with respect to the bridgehead C−C bond in **1** while *cis* in **2**), we have to conclude that this plays an important role in the stabilization of the π_L orbitals. Most of the stabilizing effect of the electron-withdrawing CO_2Me substituents is lost when they are located *cis* with respect to the bridgehead C−C bond.

Electrochemistry of 4. Figure 6 shows a voltammogram for the reduction and reoxidation of the mercurial compound **4** in PC. In the first cathodic-going scan, a reduction peak A is observed at −1.06 V. Upon scan reversal, an oxidation peak B is obtained at −0.34 V, but a small peak C is also detected at ca. −0.68 V. On the second scan, a new cathodic peak D appears at −0.75 V, while peak A diminishes. Subsequent scans show that peaks C and D continously grow and represent an electrochemical couple.

It is interesting to notice the similarity between the first cycle voltammogram of **4** and those of **1** and **2**. This suggests the idea that oxidations and reductions imply charge transfers from or toward the same kind of molecular orbitals. On the other hand, E_p for the reduction of **4** is located at −1.06 V, while that of **1** and **2** takes place at −1.2 V (in PC). Thus, this difference of 0.14 eV (ca. 13.5 kJ mol^{-1}) can be associated with the longer distance between both Mo atoms caused by the presence of Hg in the middle.

It seems that the presence of the Hg atom gives rise to a higher separation between both Mo rather than to a drastic molecular orbital (MO) change. In this way, the longer Mo−Mo distance allows their interaction with the Cp rings without demanding an excessive loss of coplanarity and, then, in conjugation in the Fv group.

An ECE mechanism is proposed for the reduction of **4**, as for **1** and **2** and related compounds,[32] which can be represented by the following scheme:

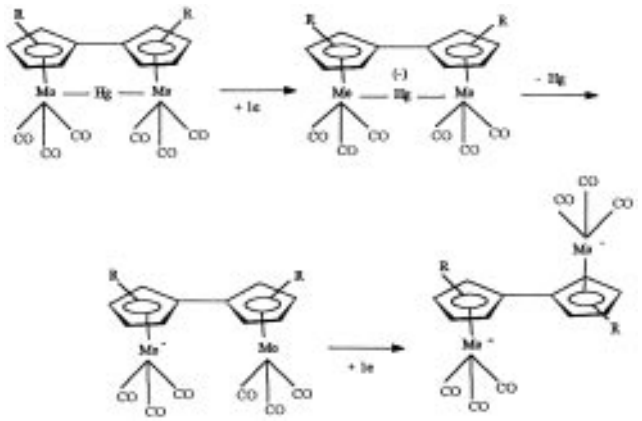

The chemical step in the mechanism involves the breaking of the Mo−Hg−Mo interaction with the subsequent liberation of Hg, which adsorbs on the electrode surface giving rise to peaks C and D. The doubly reduced Mo species is the same as that obtained for the nonmercurial compound, in agreement with the reoxidation peak appearing at nearly the same potential (Table 6).

The consecutive voltammograms recorded in Figure 6 support the proposed mechanism. Thus, peak A corresponding to the first reduction in the ECE sequence systematically decreases in each cycle, as the compound is decomposed, while peaks C and D correspondingly grow, as Hg gets free after each decomposing reduction carried out at each cathodic semicycle.

As for the oxidation peak of **4**, it is located at +0.66 V, more positive than the corresponding peak in the parent compound **2** (+0.56 V). These electrochemical data are in agreement with a situation in which both Cp rings in the Fv of **4** are orientated in a way which allows a higher conjugation, with the consequence of a higher stabilization of the electrons occupying the π orbitals.

Correlation between Electrochemical and Spectrochemical Data. Diagram of Molecular Energy Levels for 1. The electrochemical oxidation and reduction potentials gathered in Table 6 can be put together with the transitions ascribed for the UV spectrum of **1** in order to locate the MO in the energy scale. The standard electrode potential of H^+/H_2 has been converted into the physical energy scale by means of the factor of Lohman,[35] according to which $E°(H^+/H_2) = -4.5$ eV. Thus, the conversion of E_p values in Table 6 leads

(35) Lohman, F. *Z. Naturforsch.* **1967**, *22a*, 843.

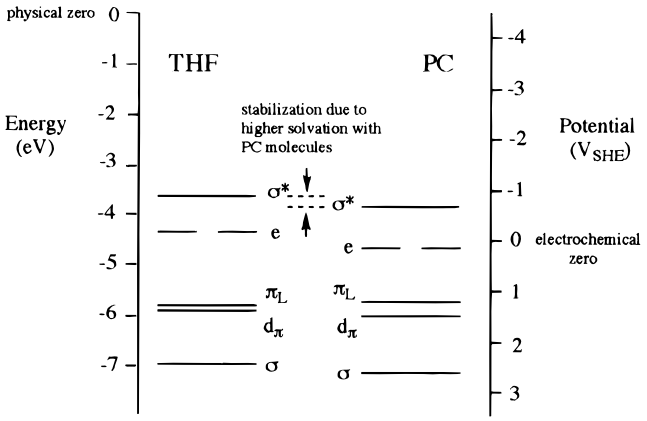

Figure 7. Diagram of molecular energy levels for **1** in THF and PC.

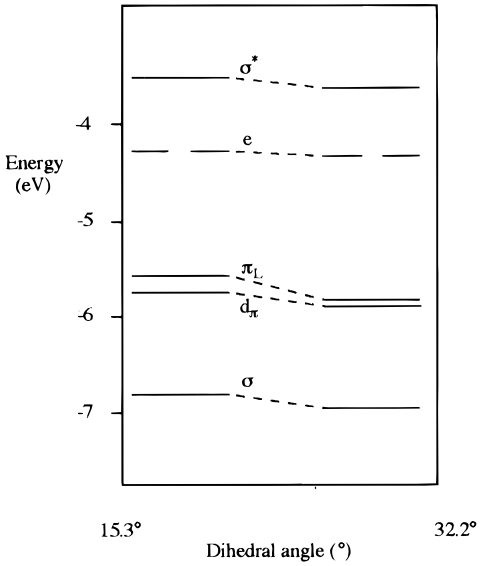

Figure 8. Walsh correlation diagram for MO levels of **1** and **5** in THF.

to the MO diagram given in Figure 7 for **1** in THF and PC. As discussed, the reduction **1** → $\mathbf{1}^{2-}$ corresponds to charge transfers from the electrode to the σ^* metal−metal antibonding orbital. Thus, a nonradiative electron transfer should take place when the Fermi level in the electrode reaches the energy corresponding to the unoccupied σ^* orbital, which is close to E_p, i.e. at −1.37 V vs Fc^+/Fc (−0.82 V_{SHE}, −3.68 eV in the physical scale) in THF and −1.20 V vs Fc^+/Fc (−0.65 V_{SHE}, −3.85 eV) in PC.

On the other hand, the UV spectrum shows a band at 378 nm (3.28 eV) in THF and at 380 nm (3.26 eV) in PC, which is attributed to the $\sigma \rightarrow \sigma^*$ transition.[1,27] This means that the σ metal−metal bonding orbital is located 3.28 and 3.26 eV below σ^* in THF and PC, respectively (at −6.96 eV for THF and −7.11 eV for PC). Furthermore, since a second band in the UV spectrum is attributed to the $d_\pi \rightarrow \sigma^*$ transition[1,27] and appears at 565 nm (2.19 eV) both in THF and PC, the d_π orbital can be located at an intermediate level between σ and σ^*, i.e. 1.09 eV over the σ orbital (−5.87 eV in THF and −6.02 eV in PC).

The reoxidation peak $\mathbf{1}^{2-} \rightarrow \mathbf{1}$ is attributed to the loss of two electrons by the doubly reduced compound, which probably has adopted a trans-configuration. Therefore, the electrons are extracted from $Mo(CO)_3$ doubly occupied and degenerated metal centered orbitals (probably e type in a C_{3v} configuration[36]).[36] After the removal of one electron, a ↑↓ ↑ configuration is left and a reorganization reaction with a twist of the molecule around the σ bond between both rings takes place, allowing the interaction between the e orbitals of both individual Mo atoms to produce the σ and σ^* metal−metal orbitals, first relaxed and finally strained after a second charge transfer, inverting in this way the ECE process for the reduction. Thus, the location of the reoxidation peaks in the potential scale enables to determine the energy of the e orbitals corresponding to the C_{3v} configuration of individual $Mo(CO)_3$ components of the whole molecule. They result to be located at −0.15 V_{SHE} (−4.35 eV) in THF and at +0.16 V_{SHE} (−4.66 eV) in PC.

Finally, the oxidation process has been diagnosed to take place due to charge transfer from the π bonding orbital of Fv (or, in any case, from a ligand-localized orbital) toward the electrode, since no influence of a change in the metal center on the oxidation potential was observed for related compounds.[32] The high positive potential value indicates the high stability of this orbital and suggests that conjugation is probably playing a role. The π_L bonding ligand-localized orbital can be located at +1.30 V_{SHE} (−5.8 eV) for THF and at +1.20 V_{SHE} (−5.7 eV) in PC. The small difference observed between both solvents (oxidation demands a potential 0.1 V less positive in PC) can be related to the stabilization of the cation radical formed through solvation with the more polar PC molecules. These results and MO assignments are summarized in Figure 7.

The irreversible oxidation of these compounds should be the consequence of the loss of donating character of the Fv rings induced by the removal of electrons from their π_L orbitals with the formation of cationic radicals. In this case, the donating character of the solvent molecules allows them to compete with the ligands to substitute them in the first solvation or ligand sphere, with the consequence of the formation of a new compound. Therefore, the nature of the voltammetric wave can be diagnosed as an EC mechanism, i.e. an electrochemical charge transfer followed by the chemical substitution of ligands by solvent molecules in the bonding sphere of the complex.

The stabilazing effect of the carbomethoxy substituents in the Fv rings on the energy of the molecular orbitals is shown in the Walsh correlation diagram of Figure 8. Energy levels of the unsubstituted compound **5** have been calculated by using electrochemical and UV−visible spectroscopy data in a similar way to that employed for **1**.

Acknowledgment. We express our great appreciation of financial support from the DGICYT (Project PB 91-0003) of Spain. We thank Dr. M. Teresa Sevilla Escribano for the Hg analysis and Dr. Ernesto Brunet for the ^{199}Hg NMR spectra.

Supporting Information Available: Tables of crystallographic parameters, positional and thermal parameters, and complete bond distances and angles for **1** and **2** (12 pages). Ordering information is given on any current masthead page.

OM960405L

(36) Thorn, D. L.; Hoffmann, R. *Inorg. Chem.* **1978**, *17*, 126.